Optimized Construction of Reed-Solomon Coded Cooperative MIMO System Based on Network Coding

Chunli ZHAO [1], Fengfan YANG [2], Binkun LIU [1], Hongjun XU [3]

[1] College of Information Science and Engineering, Henan University of Technology, Zhengzhou, 450001 China
[2] College of Electronics and Information Engg., Nanjing Univ. of Aeronautics and Astronautics, Nanjing, 210016 China
[3] School of Engineering, University of KwaZulu-Natal, King George V Avenue, Durban, 4041, South Africa

chunlizhao_cn@163.com, yffee@nuaa.edu.cn, bkliu@haut.edu.cn, xuh@ukzn.ac.za

Submitted August 17, 2025 / Accepted October 19, 2025 / Online first December 12, 2025

Abstract. *To significantly enhance the reliability and spectral efficiency of small data block transmission, this paper presents a novel network-coding-based Reed-Solomon coded cooperative multiple-input multiple-output (NC-RSCC-MIMO) system. The system consists of two single-antenna source nodes operating in full-duplex mode and one multi-antenna destination node, where the sources achieve cooperation through network coding, enabling the destination to generate two equivalent linear block codes. In the NC-RSCC-MIMO system, the selection method of network coding coefficient combination (NCCC) influences the codeword weight distribution of the equivalent codes at the destination. In order to optimize the codeword weight distribution for enhanced system construction, this paper proposes two optimized algorithms, i.e., optimal NCCC selection (ONCCCS) and low-complexity optimized NCCC selection (LC-ONCCCS) algorithms. Also, leveraging the parallel feature of the proposed NC-RSCC-MIMO system, a joint RS decoding strategy is designed at the destination to achieve efficient decoding of the two equivalent codes. Monte Carlo simulations show both ONCCCS and LC-ONCCCS algorithms improve error performance with minimal difference between them, and provide better performance gains over the random NCCC selection algorithm. The results also indicate that the NC-RSCC-MIMO system outperforms non-cooperative and existing counterparts by larger than 1.1 dB and 1 dB, respectively.*

Keywords

Reed-Solomon (RS) codes, coded cooperation, Multiple-Input Multiple-Output (MIMO), network coding, optimized network coding coefficient combination selection

1. Introduction

Cooperative communication is an effective technique for mitigating channel fading, whose fundamental principle involves forming a virtual multi-antenna system through coordinated transmission among distributed nodes [1]. Thus, it can achieve equivalent spatial diversity gain without requiring physical multi-antenna configurations. The key mechanism of cooperative communication lies in the signal regeneration processing at relay nodes, with three primary protocols: amplify-and-forward (AF) [2], compress-and-forward (CF) [3] and decode-and-forward (DF) [4]. The AF protocol directly amplifies received signals, offering implementation simplicity at the cost of noise accumulation. Under CF operation, the intermediary node first receives the original transmission and then forwards a compressed version to the endpoint. The DF protocol performs digital demodulation or decoding before retransmission, effectively suppressing noise propagation and consequently emerging as the most widely adopted protocol. In mobile wireless communication environments, transmitted signals typically face dual challenges, i.e., superimposed interference of channel noise and multipath fading effects. To address the suppression of additive noise, the academic community widely adopts a strategy combining channel codes with cooperative communication, thereby giving rise to coded cooperative technology [5]. Compared with point-to-point non-cooperative systems, coded cooperative technology can achieve cooperative diversity gain. Currently, turbo, low-density parity-check (LDPC) and polar coded cooperation [6–10] have been extensively investigated. However, these techniques generally achieve better bit error rate (BER) performance only under long information lengths, thus failing to adequately meet the requirements of emerging practical communication scenarios such as device-to-device (D2D) communication [11], [12], cellular networks [13] and vehicle-to-vehicle networks [14].

Fortunately, the well-known short-length Reed-Solomon (RS) codes exhibit maximum distance separable properties, relatively low encoding/decoding complexity, and excellent capabilities for correcting both random and burst errors [15]. Consequently, this has prompted researchers to focus on coded cooperation adopting short-length RS codes. For example, a hybrid coding architecture combining RS and convolutional codes in dual-source cooperative communications were investigated in [16],

DOI: 10.13164/re.2025.0710

effectively mitigating noise interference effects. The study in [17] presented a novel RS coded cooperative system employing relay information selection, where simulations showed optimized relay selection outperformed random selection in system performance. In [18], the authors further investigated relay information selection algorithms for the RS coded cooperative system. While maintaining the exhaustive search algorithm identical to [17], a modified partial search algorithm was also proposed. Numerical results validated the effectiveness of both the optimized algorithms. In [19], the academic researchers innovatively incorporated a special multiple-input multiple-output (MIMO) technique, i.e., spatial modulation (SM) into the RS coded cooperative system with a random selection method for the source estimation information, significantly improving spectral efficiency and BER performance. Building on this work, the authors in [20] proposed a novel relay selection algorithm on the basis of optimized codeword weight distribution at the common destination point.

However, the above studies of RS coded cooperation have key limitations: 1) The single-antenna configurations in [16–18] cannot fully exploit high spectral efficiency and diversity gain provided by MIMO. 2) The multi-antenna SM approaches in [19], [20] incur complicated antenna configurations despite improvements in spectral utilization and error performance. To overcome these challenges, this paper proposes an innovative hybrid approach that combines network coding with RS coded cooperation in the case of dual sources, maintaining high spectral efficiency through network coded algebraic properties while leveraging multi-antenna configurations of the destination to achieve better diversity gain. By allowing intermediate nodes to encode and combine received data, the robustness of the communication system is also significantly improved. The main contributions are as follows:

- This paper proposes a network-coding-based RS coded cooperative MIMO (NC-RSCC-MIMO) system, which consists of two source nodes working in full-duplex mode and one destination node. In terms of the hardware configuration, the two source nodes are each equipped with a single antenna, while the destination node adopts a multi-antenna configuration to effectively enhance the receive diversity.
- In this NC-RSCC-MIMO system, the two source nodes perform linear network coding combination on two distinct RS codewords to realize cooperation during their corresponding transmission, making the destination node construct two equivalent linear block codes. Considering the diversity of network coding coefficient combination (NCCC), an optimal NCCC selection (ONCCCS) algorithm based on exhaustive search is proposed to generate the equivalent codes with the best weight distribution for system optimization.
- As the element number of the Galois field expands and the information length becomes larger, this ONCCCS algorithm experiences substantial growth in computational complexity. To overcome this challenge, a novel low-complexity optimized NCCC selection (LC-ONCCCS) algorithm by local search is proposed.
- Additionally, for the equivalent codes constructed at the destination, a parallel joint RS decoding strategy is designed to more efficiently achieve both the coding gain (provided by the equivalent codes) and cooperative diversity gain.

This paper is structured as follows. The transmission framework of the NC-RSCC-MIMO system is thoroughly analyzed in Sec. 2. Section 3 introduces two proposed optimized NCCC selection algorithms (i.e., ONCCCS and its low-complexity variant LC-ONCCCS) to improve codeword weight distribution, thereby achieving system optimization. The methodology of the innovative parallel joint RS decoding strategy is comprehensively described in Sec. 4. The system performance evaluation via numerical simulations is presented in Sec. 5, followed by concluding remarks in Sec. 6.

Notation: Vector quantities are denoted by bold lowercase letters, while matrices are represented by bold uppercase letters. Scalar values appear in regular font, with italic letters indicating variables. Mathematical operations include: $[\cdot]^{\mathrm{T}}$ for vector/matrix transpose, and $CN(a,b)$ for complex Gaussian distribution with mean a and variance b. The notation $|\mathbf{a}|\mathbf{b}|$ denotes the concatenation of elements $\mathbf{a}$ and $\mathbf{b}$, $|S|$ indicates the cardinality of the set S, $\min(\cdot)$ is the minimum value function, $\lfloor\cdot\rfloor$ denotes the floor operator and C_a^b is the binomial coefficient.

2. Network-Coding-Based RS Coded Cooperative MIMO (NC-RSCC-MIMO) System

This paper proposes a NC-RSCC-MIMO system that has two single-antenna source nodes (S_1 and S_2) and a destination node D with n_{r} antennas, as depicted in Fig. 1. Notably, the communication system comprises two similar transmission processes, each spanning two time slots. The first process includes $S_1 \to S_2$, $S_1 \to D$ and $S_2 \to D$ channel links, while the second process consists of $S_2 \to S_1$, $S_2 \to D$ and $S_1 \to D$ channel links. During the first process, the source node S_2 acts as the network node and performs network coding on both the data packets received from S_1 and its own locally generated data packets. In the second process, the source node S_1 serves as the network node, and combines data packets received from S_2 with its local data packets for network coding. Through network coding, the source nodes realize mutual cooperation, which makes two equivalent linear block codes be constructed in the destination node. By performing parallel joint RS decoding on the equivalent codes, the source message sequences are further effectively retrieved. It should be specifically noted that although the proposed NC-RSCC-MIMO system maintains

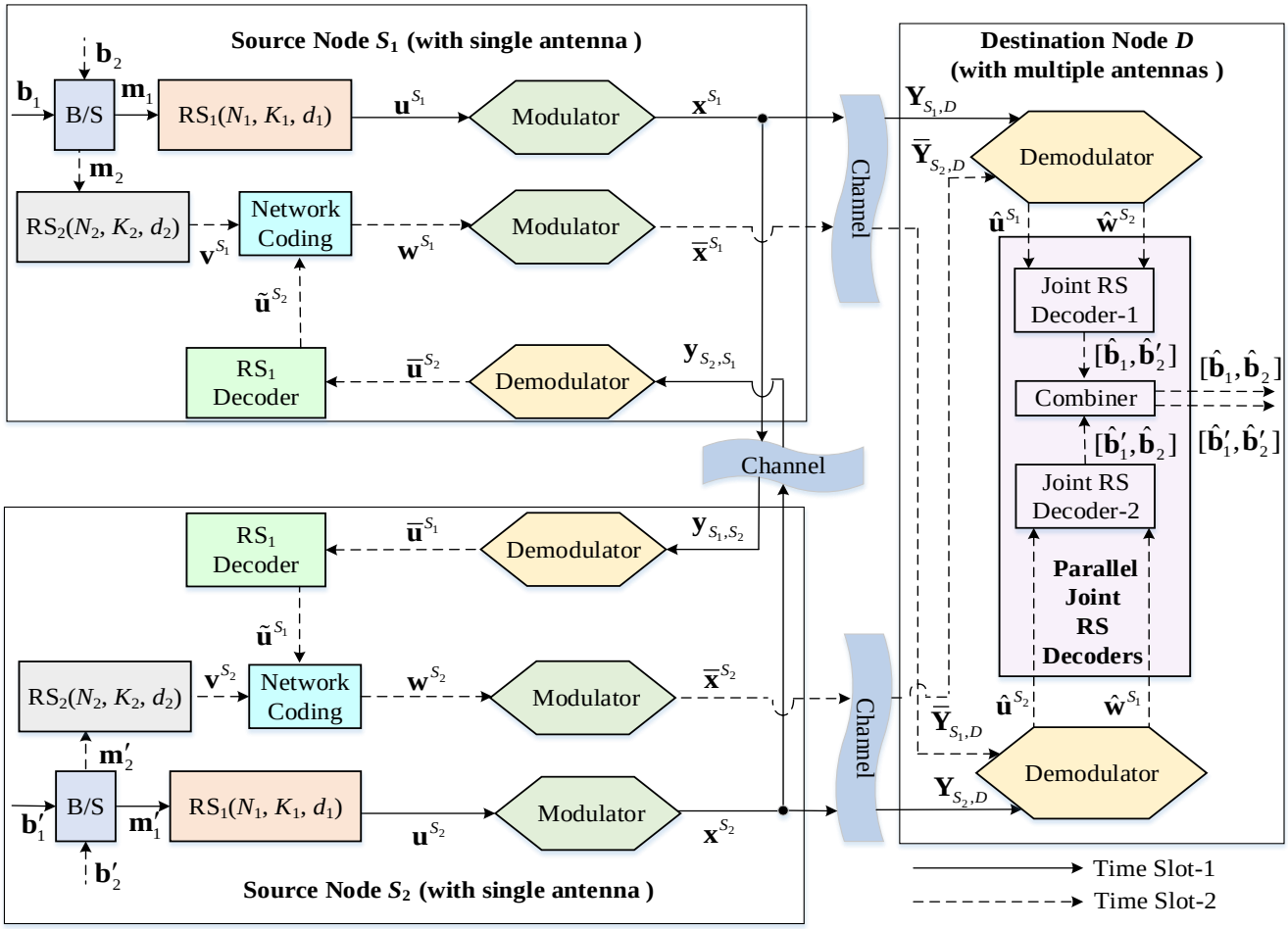

Fig. 1. System model of the NC-RSCC-MIMO.

continuity with existing works [17–20] in its application of RS codes, it achieves fundamental innovations across the technical roadmap. Specifically: 1) In terms of system architecture, it evolves from the traditional three-node model with a dedicated relay (i.e., the model composed of source, relay and destination) to an integrated cooperative model where dual-source nodes have relay functionality. 2) Regarding technology integration, the combination of network coding with cooperative and MIMO techniques (using two single-antenna sources and a multi-antenna destination) achieves high spectral efficiency and superior error performance while maintaining low complexity, thereby overcoming the limitations (of spectral efficiency and performance) of the single-antenna configurations in [17], [18] and avoiding the high-complexity drawbacks of the SM schemes in [19], [20]. 3) At the core algorithm level, it progresses from optimizing the information symbol selection at the relay to optimizing the NCCC selection in the sources. 4) In joint decoding at the destination, it evolves from traditional joint decoding to a novel joint parallel decoding designed for the equivalent codes generated by network coding.

First, the first communication transmission process (i.e., $S_1 \to S_2$, $S_1 \to D$ and $S_2 \to D$) with two time slots is described. **(1)** During time slot-1, the length-k_1 information bit sequence $\mathbf{b}_1 = [b_{1,1}, b_{1,2},\ldots, b_{1,k_1}]$ over the Galois field GF(2) at the source node S_1 is converted into a length-K_1 symbol sequence $\mathbf{m}_1 = [m_{1,1}, m_{1,2},\ldots, m_{1,K_1}]$ over the Galois field $\mathrm{GF}(2^m) = \{0,1,\alpha,\ldots,\alpha^{2^m-2}\}$ by the bits-to-symbols (B/S) module, where $K_1 = k_1 / m$ ($m > 1$), α is a primitive element, and each element $m_{1,i}$ corresponds to the m-bit vector $b_{1,mi'-(m-1)}, b_{1,mi'-(m-1)+1},\ldots,b_{1,mi'}$ for $i' = 1,2,\ldots,K_1$. $\mathbf{m}_1$ is encoded into systematic codeword symbol sequence $\mathbf{u}^{S_1} = [u_1^{S_1}, u_2^{S_1},\ldots,u_{N_1}^{S_1}]$ by the RS code $\mathrm{RS}_1(N_1,K_1,d_1)$ over $\mathrm{GF}(2^m)$with the code dimension K_1, codeword length N_1 and minimum distance $d_1 = N_1 - K_1 + 1$. The codeword polynomial $\mathbf{u}^{S_1}(x) = u_1^{S_1} + u_2^{S_1}x + \ldots + u_{N_1}^{S_1}x^{N_1-1}$ of $\mathbf{u}^{S_1}$ is [19]

$$\mathbf{u}^{S_1}(x) = x^{N_1-K_1}\mathbf{m}_1(x) + \mathbf{p}_1(x) \tag{1}$$

where $\mathbf{m}_1(x) = m_{1,1} + m_{1,2}x + \ldots + m_{1,K_1}x^{K_1-1}$ stands for the polynomial of the information symbol sequence $\mathbf{m}_1$ and $\mathbf{p}_1(x) = p_{1,1} + p_{1,2}x + \ldots + p_{1,N_1-K_1}x^{N_1-K_1-1}$ denotes the parity polynomial (where $p_{1,i_1} \in \mathrm{GF}(2^m)$ for $i_1 = 1,2,\ldots,N_1-K_1$) with the following expression [19]:

$$\mathbf{p}_1(x) = x^{N_1-K_1}\mathbf{m}_1(x) / \mathbf{g}_1(x) \tag{2}$$

where $\mathbf{g}_1(x)$ denotes the generator polynomial (with $N_1 - K_1$ consecutive roots α, α^2,..., $\alpha^{N_1-K_1}$) of $\mathrm{RS}_1(N_1,K_1,d_1)$ and is represented as [17]

$$\begin{aligned}\mathbf{g}_1(x) &= (x-\alpha)(x-\alpha^2)...(x-\alpha^{N_1-K_1}) \\ &= g_{1,1} + g_{1,2}x + ... + g_{1,N_1-K_1+1}x^{N_1-K_1}\end{aligned} \tag{3}$$

where $g_{1,j_1} \in \mathrm{GF}(2^m)$ ($j_1 = 1,2,\ldots,N_1-K_1+1$). The codeword sequence $\mathbf{u}^{S_1}$ is further fed into the M-ary quadrature-amplitude modulation (M-QAM) modulator to generate the modulated signal $\mathbf{x}^{S_1} = [x_1^{S_1}, x_2^{S_1},\ldots, x_{N_1}^{S_1}]$ of length N_1, where $M = 2^m$. Table 1 presents how each element in the finite Galois field $\mathrm{GF}(2^4) = \{0,1,\beta,\beta^{14}\}$ is mapped onto 16-QAM modulated constellation symbol, where β is the root of the primitive polynomial $1 + x + x^4$ over GF(2). Subsequently, the modulated symbol sequence $\mathbf{x}^{S_1}$ is transmitted from S_1 to S_2 via the S_1 - S_2 channel and to the destination node D via the S_1 - D channel. At the t_1^{th} ($t_1 = 1,2,\ldots,N_1$) time instant, the corresponding received signals $y^{t_1}_{S_1,S_2}$ (at the S_2) and $\mathbf{y}^{t_1}_{S_1,D}$ (at the D) are denoted as follows:

$$y^{t_1}_{S_1,S_2} = h^{t_1}_{S_1,S_2} x^{S_1}_{t_1} + n^{t_1}_{S_1,S_2}, \tag{4}$$

$$\mathbf{y}^{t_1}_{S_1,D} = \mathbf{h}^{t_1}_{S_1,D} x^{S_1}_{t_1} + \mathbf{n}^{t_1}_{S_1,D} \tag{5}$$

where $h^{t_1}_{S_1,S_2}$ and $\mathbf{h}^{t_1}_{S_1,D} = [h^{t_1,1}_{S_1,D}, h^{t_1,2}_{S_1,D},..., h^{t_1,n_r}_{S_1,D}]^{\mathrm{T}}$ denote the Rayleigh fading channels with all independent elements distributed as $CN(0,1)$. The noise $n^{t_1}_{S_1,S_2}$ follows $CN(0,\sigma_1^2)$, while each element of $\mathbf{n}^{t_1}_{S_1,D} = [n^{t_1,1}_{S_1,D}, n^{t_1,2}_{S_1,D},..., n^{t_1,n_r}_{S_1,D}]^{\mathrm{T}}$ follows $CN(0,\sigma_2^2)$. Therefore, after N_1 time instants, the received signals at the source node S_2 and the destination node D are separately represented as $\mathbf{y}_{S_1,S_2} = [y^1_{S_1,S_2}, y^2_{S_1,S_2},..., y^{N_1}_{S_1,S_2}]$ and $\mathbf{Y}_{S_1,D} = [\mathbf{y}^1_{S_1,D}, \mathbf{y}^2_{S_1,D},..., \mathbf{y}^{N_1}_{S_1,D}]$. **(2)** In time slot-2, the source node S_2 employs a demodulator to perform maximum likelihood detection (MLD) on the received signal $\mathbf{y}_{S_1,S_2}$, generating an estimate $\bar{\mathbf{u}}^{S_1}$ of the sequence $\mathbf{u}^{S_1}$. Subsequently, the RS_1 decoder processes $\bar{\mathbf{u}}^{S_1}$ and outputs an estimated codeword symbol sequence $\tilde{\mathbf{u}}^{S_1}$ by using Euclidean decoding method. This sequence $\tilde{\mathbf{u}}^{S_1}$ undergoes network coding with the systematic codeword symbol sequence $\mathbf{v}^{S_2} = [v_1^{S_2}, v_2^{S_2},..., v_{N_2}^{S_2}]$ from the RS code $\mathrm{RS}_2(N_2, K_2, d_2)$ over $\mathrm{GF}(2^m)$, where the parameters N_2 ($N_2 = N_1$), K_2 ($K_2 < K_1$) and $d_2 = N_2 - K_2 + 1$ are separately the codeword length, code dimension and minimum distance, and the corresponding polynomial $\mathbf{v}^{S_2}(x) = v_1^{S_2} + v_2^{S_2}x + \ldots + v_{N_2}^{S_2}x^{N_2-1}$ of the codeword $\mathbf{v}^{S_2}$ has the following form [19]:

$$\mathbf{v}^{S_2}(x) = x^{N_2-K_2}\mathbf{m}'_2(x) + \mathbf{p}_2(x) \tag{6}$$

where $\mathbf{m}'_2(x) = m'_{2,1} + m'_{2,2}x + \ldots + m'_{2,K_2}x^{K_2-1}$ denotes the polynomial of the information symbol sequence $\mathbf{m}'_2 = [m'_{2,1}, m'_{2,2}, \ldots, m'_{2,K_2}]$ over the Galois field $\mathrm{GF}(2^m)$ (note that the length-K_2 sequence $\mathbf{m}'_2$ is obtained by converting the length-k_2 ($k_2 = K_2 m$) information bit sequence $\mathbf{b}'_2 = [b'_{2,1}, b'_{2,2}, \ldots, b'_{2,k_2}]$ through B/S block) and $\mathbf{p}_2(x) = p_{2,1} + p_{2,2}x + \ldots + p_{2,N_2-K_2}x^{N_2-K_2-1}$ denotes the parity polynomial ($p_{2,i_2} \in \mathrm{GF}(2^m)$ for $i_2 = 1,2,\ldots,N_2-K_2$) with the following expression [19]:

$$\mathbf{p}_2(x) = x^{N_2-K_2}\mathbf{m}'_2(x) / \mathbf{g}_2(x) \tag{7}$$

where $\mathbf{g}_2(x)$ is the generator polynomial (with $N_2 - K_2$ consecutive roots $\alpha,\alpha^2,\ldots,\alpha^{N_2-K_2}$) of $\mathrm{RS}_2(N_2, K_2, d_2)$ and represented as [17]

$$\begin{aligned}\mathbf{g}_2(x) &= (x-\alpha)(x-\alpha^2)...(x-\alpha^{N_2-K_2}) \\ &= g_{2,1} + g_{2,2}x + ... + g_{2,N_2-K_2+1}x^{N_2-K_2}\end{aligned} \tag{8}$$

where $g_{2,j_2} \in \mathrm{GF}(2^m)$ for $j_2 = 1,2,\ldots,N_2-K_2+1$. Then, the sequence $\mathbf{w}^{S_2} = \alpha_1^{(i)}\tilde{\mathbf{u}}^{S_1} + \alpha_2^{(i)}\mathbf{v}^{S_2} = [w_1^{S_2}, w_2^{S_2},..., w_{N_2}^{S_2}]$ (network-coded sequence) of length N_2 is further generated, in which $\alpha_1^{(i)}, \alpha_2^{(i)} \in \mathrm{GF}(2^m)$, $(\alpha_1^{(i)}, \alpha_2^{(i)})$ is the NCCC and i ($1 \le i \le (2^m)^2 = 4^m$) is the NCCC selection index. It should be noted that different NCCCs directly impact the weight distribution of the equivalent code at the D, making their proper selection crucial. The details of the optimized NCCC selection algorithms are presented in Sec. 3. Through the M-QAM modulator, $\mathbf{w}^{S_2}$ is modulated into the symbol sequence $\bar{\mathbf{x}}^{S_2} = [\bar{x}_1^{S_2}, \bar{x}_2^{S_2},..., \bar{x}_{N_2}^{S_2}]$ of length N_2. Subsequently, $\bar{\mathbf{x}}^{S_2}$ is transmitted to the destination D via the S_2-D channel, and the received sequence at the t_2-th ($t_2 = 1,2,\ldots,N_2$) time instant is denoted as

$$\bar{\mathbf{y}}^{t_2}_{S_2,D} = \bar{\mathbf{h}}^{t_2}_{S_2,D}\bar{x}^{S_2}_{t_2} + \bar{\mathbf{n}}^{t_2}_{S_2,D} \tag{9}$$

where $\bar{\mathbf{h}}^{t_2}_{S_2,D} = [\bar{h}^{t_2,1}_{S_2,D}, \bar{h}^{t_2,2}_{S_2,D},..., \bar{h}^{t_2,n_r}_{S_2,D}]^{\mathrm{T}}$ represents the Rayleigh fading channel with all independent elements following $CN(0, 1)$

Field elements	4-bit vector	Modulated symbols
0	[0, 0, 0, 0]	−3 + 3i
1	[1, 0, 0, 0]	3 + 3i
β	[0, 1, 0, 0]	−1 + 3i
β^2	[0, 0, 1, 0]	−3 − 3i
β^3	[0, 0, 0, 1]	−3 + i
β^4	[1, 1, 0, 0]	1 + 3i
β^5	[0, 1, 1, 0]	−1 − 3i
β^6	[0, 0, 1, 1]	−3 − i
β^7	[1, 1, 0, 1]	1 + i
β^8	[1, 0, 1, 0]	3 − 3i
β^9	[0, 1, 0, 1]	−1 + i
β^{10}	[1, 1, 1, 0]	1 − 3i
β^{11}	[0, 1, 1, 1]	−1 − i
β^{12}	[1, 1, 1, 1]	1 − i
β^{13}	[1, 0, 1, 1]	3 − i
β^{14}	[1, 0, 0, 1]	3 + i

Tab. 1. Mapping process of each element in $\mathrm{GF}(2^4)$ to 16-QAM modulated symbol.

and each element of $\bar{\mathbf{n}}_{S_2,D}^{t_2} = [\bar{n}_{S_2,D}^{t_2,1}, \bar{n}_{S_2,D}^{t_2,2}, ..., \bar{n}_{S_2,D}^{t_2,n_r}]^{\mathrm{T}}$ obeying $CN(0, \sigma_3^2)$. Therefore, after N_2 time instants, the received signal at the D is $\bar{\mathbf{Y}}_{S_2,D} = [\bar{\mathbf{y}}_{S_2,D}^1, \bar{\mathbf{y}}_{S_2,D}^2, ..., \bar{\mathbf{y}}_{S_2,D}^{N_2}]$. The demodulator carries out the demodulation for the received signals $\mathbf{Y}_{S_1,D}$ and $\bar{\mathbf{Y}}_{S_2,D}$ to generate the estimate (i.e., $\hat{\mathbf{u}}^{S_1}$ and $\hat{\mathbf{w}}^{S_2}$) of $\mathbf{u}^{S_1}$ and $\mathbf{w}^{S_2}$, respectively. The joint RS decoder-1 of the parallel joint RS decoders processes the estimate $|\hat{\mathbf{u}}^{S_1}|\hat{\mathbf{w}}^{S_2}|$ of the codeword $|\mathbf{u}^{S_1}|\mathbf{w}^{S_2}|$ in the equivalent code $C_D^{(i)}(N_1+N_2, K_1+K_2)$ to obtain the estimate of the bit sequences $\mathbf{b}_1$ (from the S_1) and $\mathbf{b}'_2$ (from the S_2). The details of the joint decoding will be introduced in Sec. 4.

Next, the second transmission process (i.e., $S_2 \to S_1$, $S_2 \to D$ and $S_1 \to D$) is described, which is analogous to the first transmission process (i.e., $S_1 \to S_2$, $S_1 \to D$ and $S_2 \to D$). Here, the key differences between this process and the first process are highlighted: 1) The source node S_1 is the network node and the network-coded sequence generated at this node is mathematically formulated as $\mathbf{w}^{S_1} = \bar{\alpha_1}^{(i)} \tilde{\mathbf{u}}^{S_2} + \bar{\alpha_2}^{(i)} \mathbf{v}^{S_1} = [w_1^{S_1}, w_2^{S_1}, ..., w_{N_1}^{S_1}]$, in which the definitions of $\tilde{\mathbf{u}}^{S_2}$ and $\mathbf{v}^{S_1}$ can refer to those of $\tilde{\mathbf{u}}^{S_1}$ and $\mathbf{v}^{S_2}$, and the definition of $(\bar{\alpha_1}^{(i)}, \bar{\alpha_2}^{(i)})$ is similar to $(\alpha_1^{(i)}, \alpha_2^{(i)})$. 2) The joint decoder-2 at the D processes the estimate $|\hat{\mathbf{u}}^{S_2}|\hat{\mathbf{w}}^{S_1}|$ of the codeword $|\mathbf{u}^{S_2}|\mathbf{w}^{S_1}|$ in the equivalent code $C'^{(i)}_D(N_1+N_2, K_1+K_2)$ to obtain the estimate of the bit sequences $\mathbf{b}'_1$ (from the S_2) and $\mathbf{b}_2$ (from the S_1), where the definitions of $\mathbf{b}'_1$, $\mathbf{b}_2$, $\mathbf{u}^{S_2}$ and $\mathbf{w}^{S_1}$ can refer to those of $\mathbf{b}_1$, $\mathbf{b}'_2$, $\mathbf{u}^{S_1}$ and $\mathbf{w}^{S_2}$. Section 4 will introduce the detailed decoding process.

3. Optimized Network Coding Coefficient Combination Selection Algorithms Based on Exhaustive/Local Search

Distinct NCCCs in Fig. 1 yield different equivalent linear block codes at the D, whose weight distribution critically determine BER performance. This indicates that random selection from NCCCs may lead to bad weight distribution at the D, thereby degrading communication reliability. To mitigate this issue, this section presents two optimized NCCC selection algorithms, i.e., ONCCCS and LC-ONCCCS. It should be noted that the following algorithms are developed under the assumption that the S_1–S_2 channel is free from interference (i.e., $\tilde{\mathbf{u}}^{S_1} = \mathbf{u}^{S_1}$ and $\tilde{\mathbf{u}}^{S_2} = \mathbf{u}^{S_2}$).

3.1 Optimal NCCC Selection (ONCCCS) Algorithm by Exhaustive Search

For the i-th ($1 \le i \le (2^m)^2 = 4^m$) NCCC $(\alpha_1^{(i)}, \alpha_2^{(i)})$ over GF(2^m) in the proposed NC-RSCC-MIMO system, the equivalent linear block codes yielded at the destination node D during the first and second communication transmission phases are formulated as follows:

$$\begin{aligned} &C_D^{(i)}(N_1+N_2, K_1+K_2) \\ &= \left\{ |\mathbf{u}^{S_1}|\mathbf{w}^{S_2}| \right\} = \left\{ |\mathbf{u}^{S_1}| \ \alpha_1^{(i)}\mathbf{u}^{S_1} + \alpha_2^{(i)}\mathbf{v}^{S_2}| \right\}, \end{aligned} \tag{10}$$

$$\begin{aligned} &C'^{(i)}_D(N_1+N_2, K_1+K_2) \\ &= \left\{ |\mathbf{u}^{S_2}|\mathbf{w}^{S_1}| \right\} = \left\{ |\mathbf{u}^{S_2}| \ \bar{\alpha}_1^{(i)}\mathbf{u}^{S_2} + \bar{\alpha}_2^{(i)}\mathbf{v}^{S_1}| \right\} \end{aligned} \tag{11}$$

where $\mathbf{u}^{S_1}, \mathbf{u}^{S_2} \in \mathrm{RS}_1(N_1, K_1, d_1)$, $\mathbf{v}^{S_1}, \mathbf{v}^{S_2} \in \mathrm{RS}_2(N_2, K_2, d_2)$. The weight distributions of $C_D^{(i)}(N_1+N_2, K_1+K_2)$ and $C'^{(i)}_D(N_1+N_2, K_1+K_2)$ are separately expressed as

$$W_D^{(i)} = \{1, N_{d_{\mathrm{free}}^{(i)}}^{(i)}, N_{d_{\mathrm{free}}^{(i)}+1}^{(i)}, \ldots, N_{N_1+N_2}^{(i)}\}, \tag{12}$$

$$W_D'^{(i)} = \{1, N'^{(i)}_{d_{\mathrm{free}}'^{(i)}}, N'^{(i)}_{d_{\mathrm{free}}'^{(i)}+1}, \ldots, N'^{(i)}_{N_1+N_2}\} \tag{13}$$

where $N_w^{(i)}$ and $N'^{(i)}_w$ separately denote the number of $|\mathbf{u}^{S_1}|\mathbf{w}^{S_2}|$ and $|\mathbf{u}^{S_2}|\mathbf{w}^{S_1}|$ of weights $d_{\mathrm{free}}^{(i)} \le w \le N_1+N_2$ and $d_{\mathrm{free}}'^{(i)} \le w \le N_1+N_2$, with $d_{\mathrm{free}}^{(i)}$ and $d_{\mathrm{free}}'^{(i)}$ representing the free distances of corresponding equivalent codes. Since this algorithm is designed under the condition that the S_1-S_2 link is not subject to any interference, the conclusions $C_D^{(i)}(N_1+N_2, K_1+K_2) = C'^{(i)}_D(N_1+N_2, K_1+K_2)$ and $W_D^{(i)} = W'^{(i)}_D$ are obtained. Consequently, the optimal NCCC obtained under the second transmission process is identical to that of the first transmission process. Thus, the ONCCCS algorithm only focuses on the first transmission process.

The core idea of the ONCCCS by exhaustive search is to identify the optimal NCCC corresponding to the best codeword weight distribution from all possible 4^m NCCCs by considering the total $2^{m(K_1+K_2)}$ source information symbol sequences $[\mathbf{m}_1, \mathbf{m}_2]$ of length K_1+K_2. The detailed steps are provided below.

Step 1: Determine the set Λ containing all 4^m NCCCs and their associated set L of 4^m selection indices, i.e.,

$$\Lambda = \{(\alpha_1^{(1)}, \alpha_2^{(1)}), (\alpha_1^{(2)}, \alpha_2^{(2)}), \ldots, (\alpha_1^{(4^m)}, \alpha_2^{(4^m)})\}, \tag{14}$$

$$L = \{1, 2, ..., 4^m\} \tag{15}$$

where $\alpha_1^{(i)}, \alpha_2^{(i)} \in \mathrm{GF}(2^m)$ for $1 \le i \le 4^m$.

Step 2: Consider all $2^{m(K_1+K_2)}$ source information symbol sequences $[\mathbf{m}_1, \mathbf{m}_2]$ of length K_1+K_2.

Step 3: For the i-th ($i \in L$) NCCC $(\alpha_1^{(i)}, \alpha_2^{(i)})$ in the set Λ, determine the equivalent linear block code $C_D^{(i)}(N_1+N_2, K_1+K_2)$ (generated by the considered source information symbol sequences in step 2) and the corresponding codeword weight distribution $W_D^{(i)}$.

Step 4: Find the minimum codeword weight (free distance) $d_{\mathrm{free}}^{(i)}$ for each $C_D^{(i)}(N_1+N_2, K_1+K_2)$ with $i \in L$.

Step 5: Compare $d_{\mathrm{free}}^{(i)}$ of $C_D^{(i)}(N_1+N_2, K_1+K_2)$ for $i \in L$ and determine the maximum value $d_{\mathrm{free}}^{\max}$.

Step 6: Initialization: $\tau = 1$, $L_\tau = L$ and $\Lambda_\tau = \Lambda$.

Step 7: If only one NCCC generates the codeword weight $d_{\text{free}}^{\max}$ at the destination D, i.e., $|\Lambda_{\tau+1}| = 1$ for $\Lambda_{\tau+1} = \{(\alpha_1^{(i)}, \alpha_2^{(i)}) | (\alpha_1^{(i)}, \alpha_2^{(i)}) \in \Lambda_\tau, i \in L_{\tau+1}\}$ related to the subset $L_{\tau+1} = \{i \mid i \in L_\tau, d_{\text{free}}^{(i)} = d_{\text{free}}^{\max}\}$ of L_τ, go to step 10.

Step 8: If there exist multiple NCCCs achieving the codeword weight $d_{\text{free}}^{\max}$ at the D, i.e., $|\Lambda_{\tau+1}| > 1$ for $\Lambda_{\tau+1} = \{(\alpha_1^{(i)}, \alpha_2^{(i)}) | (\alpha_1^{(i)}, \alpha_2^{(i)}) \in \Lambda_\tau, i \in L_{\tau+1}\}$ with the subset $L_{\tau+1} = \{i \mid i \in L_\tau, d_{\text{free}}^{(i)} = d_{\text{free}}^{\max}\}$ of L_τ, the number $N_w^{(i)}$ ($i \in L_{\tau+1}$) of codewords with the weight $d_{\text{free}}^{\max}$ is compared and determine the smallest number $N_w^{\min}$. Then, determine $\Lambda_{\tau+2} = \{(\alpha_1^{(i)}, \alpha_2^{(i)}) | (\alpha_1^{(i)}, \alpha_2^{(i)}) \in \Lambda_{\tau+1}, i \in L_{\tau+2}\}$ related to the subset $L_{\tau+2} = \{i | i \in L_{\tau+1}, N_w^{(i)} = N_w^{\min}\}$ of $L_{\tau+1}$.

Algorithm 1 The proposed ONCCCS

Input: m, K_1, K_2, N_1, N_2, NCCC $(\alpha_1^{(i)}, \alpha_2^{(i)})$ $(1 \le i \le 4^m)$ over GF(2^m).

Output: The optimal NCCC α_{opt}.

1: Determine $\Lambda = \{(\alpha_1^{(1)}, \alpha_2^{(1)}), (\alpha_1^{(2)}, \alpha_2^{(2)}), \ldots, (\alpha_1^{(4^m)}, \alpha_2^{(4^m)})\}$, $L = \{1, 2, \ldots, 4^m\}$.
2: Determine all $2^{m(K_1+K_2)}$ source information symbol sequences.
3: **for** $i = 1$ to 4^m **do**
4: Determine $C_D^{(i)}(N_1 + N_2, K_1 + K_2)$ and its free distance $d_{\text{free}}^{(i)}$.
5: **end for**
6: Determine the maximum free distance $d_{\text{free}}^{\max}$ of $d_{\text{free}}^{(1)}, d_{\text{free}}^{(2)}, \ldots, d_{\text{free}}^{(4^m)}$.
7: Set $\tau = 1$, $L_\tau = L$, $\Lambda_\tau = \Lambda$.
8: **for** $w = d_{\text{free}}^{\max}$ to $N_1 + N_2$ **do**
9: $L_{\tau+1} = \{i \mid i \in L_\tau, d_{\text{free}}^{(i)} = w\}$, $\Lambda_{\tau+1} = \{(\alpha_1^{(i)}, \alpha_2^{(i)}) | (\alpha_1^{(i)}, \alpha_2^{(i)}) \in \Lambda_\tau, i \in L_{\tau+1}\}$.
10: **if** $|\Lambda_{\tau+1}| = 1$ **then**
11: The codeword weight distribution $W_D^{(i)}$ for $i \in L_{\tau+1}$ is optimal. Determine α_{OPT} related to $W_D^{(i)}$ and break the algorithm.
12: **else**
13: For each $i \in L_{\tau+1}$, determine the number $N_w^{(i)}$ of the codewords with the codeword weight w and the smallest number $N_w^{\min}$. $L_{\tau+2} = \{i \mid i \in L_{\tau+1}, N_w^{(i)} = N_w^{\min}\}$, $\Lambda_{\tau+2} = \{(\alpha_1^{(i)}, \alpha_2^{(i)}) | (\alpha_1^{(i)}, \alpha_2^{(i)}) \in \Lambda_{\tau+1}, i \in L_{\tau+2}\}$.
14: **if** $w < N_1 + N_2$ **then**
15: **if** $|\Lambda_{\tau+2}| > 1$ **then**
16: $\tau \leftarrow \tau + 1$ and let $d_{\text{free}}^{(i)}$ be the minimum codeword weight of $C_D^{(i)}(N_1 + N_2, K_1 + K_2)$ for $i \in L_\tau$.
17: **end if**
18: **else**
19: Randomly select an element from $\Lambda_{\tau+2}$ as the optimal α_{OPT} corresponding to the best codeword weight distribution $W_D^{(i)}$ for $i \in L_{\tau+2}$, and break the algorithm.
20: **end if**
21: **end if**
22: **end for**

Step 9: Check w and $\Lambda_{\tau+2}$,

(i) If $w < N_1 + N_2$ and $|\Lambda_{\tau+2}| > 1$, increase τ and $d_{\text{free}}^{\max}$ by 1 each, let $d_{\text{free}}^{(i)}$ be the minimum codeword weight of $C_D^{(i)}(N_1 + N_2, K_1 + K_2)$ for $i \in L_\tau$, and go to step 7.

(ii) If not, i.e., $w = N_1 + N_2$ or $|\Lambda_{\tau+2}| = 1$, randomly select an element from $\Lambda_{\tau+2}$ as the optimal NCCC α_{opt} corresponding to the optimal codeword weight distribution $W_D^{(i)}$ for $i \in L_{\tau+2}$.

Step 10: The codeword weight distribution $W_D^{(i)}$ for $i \in L_{\tau+1}$ is optimal. Determine the unique NCCC α_{opt} corresponding to $W_D^{(i)}$ and terminate the algorithm.

In order to facilitate a clearer understanding of the aforementioned steps, **Algorithm 1** explains the generated process of the optimal NCCC α_{opt}.

3.2 Low-Complexity Optimized NCCC Selection (LC-ONCCCS) Algorithm by Local Search

The ONCCCS algorithm employs an exhaustive search approach, evaluating all 4^m potential NCCCs by considering all $2^{m(K_1+K_2)}$ source information symbol sequences [$\mathbf{m}_1$, $\mathbf{m}_2$]. However, as m, K_1 and K_2 increases, the computational complexity grows substantially. To address this, the LC-ONCCCS algorithm by local search is introduced, which examines only B ($B < 4^m$) candidate NCCCs instead of the full set by taking into account E ($E < 2^{m(K_1+K_2)}$) local sequences of $2^{m(K_1+K_2)}$ source information symbol sequences. From this reduced subset, an optimized NCCC is selected, ensuring an improved weight distribution while lowering computational overhead. The details are as follows:

Step 1: Determine the set $\bar{\Lambda}$ comprising B NCCCs and the set $\bar{L}$ containing B related selection indices, i.e.,

$$\bar{\Lambda} = \{(\bar{\alpha}_1^{(1)}, \bar{\alpha}_2^{(1)}), (\bar{\alpha}_1^{(2)}, \bar{\alpha}_2^{(2)}), \ldots, (\bar{\alpha}_1^{(B)}, \bar{\alpha}_2^{(B)})\}, \quad (16)$$

$$\bar{L} = \{1, 2, \ldots, B\} \quad (17)$$

where $\bar{\alpha}_1^{(i)}$, $\bar{\alpha}_2^{(i)} \in$ GF(2^m) for $1 \le i \le B$. The procedure for obtaining B NCCCs is as follows:

(i) Construct a matrix $\mathbf{C}$ of size $2^m \times 2^m$. Specifically, form a row vector $\mathbf{r}_0 = [0, 1, \alpha, \ldots, \alpha^{2^m-2}]$ using the 2^m elements $0, 1, \alpha, \ldots, \alpha^{2^m-2}$ over GF(2^m). Perform a cyclic right shift of $\mathbf{r}_0$ by k ($k = 0, 1, \ldots, 2^m - 1$) positions to obtain the vector $\mathbf{r}_k$. Then, use the vector $\mathbf{r}_k$ as the $(k+1)$-th row of the matrix $\mathbf{C}$, resulting in a $2^m \times 2^m$ matrix $\mathbf{C}$ denoted as

$$\mathbf{C} = \begin{bmatrix} 0 & 1 & \alpha & \ldots & \alpha^{2^{m-1}-2} & \ldots & \alpha^{2^m-2} \\ \alpha^{2^m-2} & 0 & 1 & \alpha & \ldots & \alpha^{2^{m-1}-2} & \ldots \\ \vdots & \vdots & \vdots & \vdots & \vdots & \vdots & \vdots \\ 1 & \alpha & \ldots & \alpha^{2^{m-1}-2} & \ldots & \alpha^{2^m-2} & 0 \end{bmatrix}. \quad (18)$$

(ii) For the j-th row ($j = 1,2,\ldots,2^m$) of the matrix $\mathbf{C}$, C_j elements are selected according to the following rules: a) For the first row ($j = 1$), C_1 elements are selected sequentially from the first element 0 to the last element α^{2^m-2}. b) For the subsequent 2^m-1 rows ($j = 2,3,\ldots,2^m$), the selection begins at the element α^{j-2} and continues through the rightmost element. c) If none of the first $\alpha^{2^{m-1}}$ elements is included in the current selection for the j-th ($j = 1,2,\ldots,2^m$) row of the matrix $\mathbf{C}$, the first element of that row is added to the selection, ensuring that at least one element from each of the first and second halves (each containing $\alpha^{2^{m-1}}$ elements) is selected. Next, C_j ($j = 1,2,\ldots,2^m$) elements in each row of the matrix $\mathbf{C}$ are selected.

(iii) For each selected C_j ($j = 1,2,\ldots,2^m$) elements of $\mathbf{C}$, two elements are chosen, where the fixed element is 0 for $j = 1$ and it is α^{j-2} for $j = 2,3,\ldots,2^m$. Based on this method, B reasonable candidate NCCCs from the total 4^m possible NCCCs are determined.

Step 2: Determine E source information symbol sequences with the following steps:

(i) From the selected C_{j_1} ($j_1 = 1,2,\ldots,K_1$) elements generated in step 1, determine its $\bar{C}_{j_1}$ ($\bar{C}_{j_1} \le C_{j_1}$) non-zero elements and select the elements from these non-zero elements to serve as the non-zero symbols of the information symbol sequence $\mathbf{m}_1$ with length K_1 at the source node S_1.

(ii) Similarly, among the chosen C_{j_2} ($j_2 = 1,2,\ldots,K_2$) elements obtained from step 1, identify its $\bar{C}_{j_2}$ ($\bar{C}_{j_2} \le C_{j_2}$) corresponding non-zero entries, from which the $\min(K_2 - j_2 + 1, \bar{C}_{j_2})$ elements are extracted to form the non-zero symbols of the length K_2 information symbol sequence $\mathbf{m}_2$ at S_2.

(iii) By combining (i) and (ii), E source information symbol sequences $[\mathbf{m}_1, \mathbf{m}_2]$ of length $K_1 + K_2$ are effectively obtained from the total $2^{m(K_1+K_2)}$ source information symbol sequences.

Step 3: The remaining steps follow steps 3–10 of the ONCCCS algorithm, ultimately an optimized NCCC α_{LC} is determined among B NCCCs obtained in step 1.

Algorithm 2 provides a comprehensive summary for the generation α_{LC} of the LC-ONCCCS algorithm.

4. Parallel Joint RS Decoding in the Destination

Since the proposed NC-RSCC-MIMO system consists of two communication transmission processes in Fig. 1, a parallel joint RS decoding scheme (as shown in Fig. 2) utilizes Euclidean algorithm to perform decoding on the estimates (i.e., $|\hat{\mathbf{u}}^{S_1}|\hat{\mathbf{w}}^{S_2}|$ and $|\hat{\mathbf{u}}^{S_2}|\hat{\mathbf{w}}^{S_1}|$) of $|\mathbf{u}^{S_1}|\mathbf{w}^{S_2}|$ and $|\mathbf{u}^{S_2}|\mathbf{w}^{S_1}|$, respectively. The decoding process comprises two similar stages: The joint RS decoder-1 is responsible for processing $\hat{\mathbf{u}}^{S_1}$ and $\hat{\mathbf{w}}^{S_2}$, while the joint RS decoder-2 handles $\hat{\mathbf{u}}^{S_2}$ and $\hat{\mathbf{w}}^{S_1}$. A detailed description of the procedure is provided below.

During the decoding process of the joint RS decoder-1, the RS_1 decoder decodes $\hat{\mathbf{u}}^{S_1}$ to generate the estimate $\hat{\mathbf{m}}_1$ of the information symbol sequence $\mathbf{m}_1$ at the S_1 (see Fig. 1), along with the corresponding codeword symbol sequence $\hat{\hat{\mathbf{u}}}^{S_1}$ of the estimate $\hat{\mathbf{m}}_1$. The network coding module

Algorithm 2 The proposed LC-ONCCCS

Input: m, K_1, K_2, N_1, N_2, $\mathrm{GF}(2^m) = \{0, 1, \alpha, \ldots, \alpha^{2^m-2}\}$.

Output: The optimized NCCC α_{LC}.

1: Form a row vector $\mathbf{r}_0 = [0, 1, \alpha, \ldots, \alpha^{2^m-2}]$.
2: **for** $k = 0$ to $2^m - 1$ **do**
  Perform a cyclic right shift of $\mathbf{r}_0$ by k ($k = 0,1,\ldots,2^m-1$) positions to obtain the vector $\mathbf{r}_k$.
3: **end for**
4: Construct a matrix $\mathbf{C} = [\mathbf{r}_0, \mathbf{r}_1, \ldots, \mathbf{r}_{2^m-1}]$ of size $2^m \times 2^m$.
5: For the 1st row of $\mathbf{C}$, C_1 elements $0, 1, \alpha, \ldots, \alpha^{2^m-2}$ are selected.
6: **for** $j = 1$ to 2^m **do**
7: **if** $j = 1$ **then**
8: Obtain C_j elements $0, 1, \alpha, \ldots, \alpha^{2^m-2}$. Two elements are chosen from the C_j elements to get B_j candidate NCCCs, in which the fixedly selected element is 0.
9: **else**
10: For the j-th row of $\mathbf{C}$, selection begins at the element α^{j-2} and continues through the rightmost element.
11: **if** none of the 1st $\alpha^{2^{m-1}}$ elements are in the selection **then**
12: The 1st element in the j-th row of $\mathbf{C}$ is added to the selection, and C_j elements are obtained. Select two elements from the C_j elements to generate B_j candidate NCCCs, in which the fixedly selected element is α^{j-2}.
13: **end if**
14: **end if**
15: **end for**
16: Determine $B = B_1 + B_2 + \ldots + B_{2^m}$ NCCCs from 4^m possible NCCCs.
17: Determine $\bar{L} = \{1, 2, \ldots, B\}$.
18: **for** $j_1 = 1$ to K_1 **do**
19: From the selected C_{j_1} elements, determine its $\bar{C}_{j_1}$ non-zero elements and select the $\min(j_1 - K_1 + 1, \bar{C}_{j_1})$ elements from these non-zero elements to serve as the non-zero symbols of $\mathbf{m}_1$ at S_1.
20: **end for**
21: **for** $j_2 = 1$ to K_2 **do**
22: From the chosen C_{j_2} elements, identify its $\bar{C}_{j_2}$ non-zero entries, from which the $\min(j_2 - K_2 + 1, \bar{C}_{j_2})$ elements are extracted to form the non-zero symbols of $\mathbf{m}_2$ at S_2.
23: **end for**
24: Determine E source information symbol sequences $[\mathbf{m}_1, \mathbf{m}_2]$ of length $K_1 + K_2$ from the total $2^{m(K_1+K_2)}$ information sequences.
25: Apply steps 3-10 of **Algorithm 1** to get an optimized NCCC α_{LC}.

then performs a linear combination operation $\alpha_1^{(i)}(\alpha_2^{(i)})^{-1}\hat{\tilde{\mathbf{u}}}^{S_1}+(\alpha_2^{(i)})^{-1}\hat{\mathbf{w}}^{S_2}$ on the obtained $\hat{\tilde{\mathbf{u}}}^{S_1}$ and $\hat{\mathbf{w}}^{S_2}$, generating the estimate $\hat{\mathbf{v}}^{S_2}$ of the codeword symbol sequence $\mathbf{v}^{S_2}$ at the S_2. This estimated sequence undergoes further decoding by the RS_2 decoder to ultimately obtain the estimate $\hat{\mathbf{m}}_2'$ of the information symbol sequence $\mathbf{m}_2'$ at the S_2. Finally, the symbols-to-bits (S/B) module converts $\hat{\mathbf{m}}_1$ and $\hat{\mathbf{m}}_2'$ into the bit sequences $\hat{\mathbf{b}}_1$ and $\hat{\mathbf{b}}_2'$, which serve as the final estimates for the information bit sequence $\mathbf{b}_1$ at the S_1 and the information bit sequence $\mathbf{b}_2'$ at the S_2.

The joint RS decoder-2 employs a decoding procedure analogous to that of the joint RS decoder-1, generating the estimated sequences $\hat{\mathbf{b}}_1'$ and $\hat{\mathbf{b}}_2$ for the information bit sequence $\mathbf{b}_1'$ at the S_2 and the information bit sequence $\mathbf{b}_2$ at the S_1, respectively. The combiner processes four estimated sequences $\hat{\mathbf{b}}_1$, $\hat{\mathbf{b}}_2'$, $\hat{\mathbf{b}}_1'$ and $\hat{\mathbf{b}}_2$ by reorganization, forming two new merged sequence pairs, i.e., $[\hat{\mathbf{b}}_1, \hat{\mathbf{b}}_2]$ and $[\hat{\mathbf{b}}_1', \hat{\mathbf{b}}_2']$. The first pair serves as the final estimate for the information bit combination $[\mathbf{b}_1, \mathbf{b}_2]$ at the S_1, while the second pair forms the final estimate of the information bit combination $[\mathbf{b}_1', \mathbf{b}_2']$ at the S_2.

5. Simulation Results

This section examines the BER performance of the proposed NC-RSCC-MIMO system and its comparative systems in Rayleigh fading channels. In Sec. 5.2, the performance of the proposed system under additive white Gaussian noise (AWGN) channel is employed as a benchmark and compared against its performance under Rayleigh fading channels. For AWGN channel, it has a constant gain. In the case of slow Rayleigh fading, the channel stays unchanged throughout the transmission interval of a codeword but changes between different codewords. Conversely, fast Rayleigh fading channel varies for each transmitted modulated signal. The fading coefficients in both slow and fast Rayleigh fading channel models follow $CN(0,1)$. The Rayleigh fading channel models are flat and thus free from inter-symbol interference. This approach allows clearer identification of the intrinsic relationship between system parameters and error performance. Table 2 displays the encoding parameters of three RS code pairs $RS_1(N_1, K_1, d_1)$ and $RS_2(N_2, K_2, d_2)$, their optimized NCCCs generated by the proposed ONCCCS and LC-ONCCCS algorithms, the adopted finite fields and the corresponding primitive polynomials for each Galois field, where β, λ and η correspond to the roots of $1+x+x^4$, $1+x^2+x^5$ and $1+x+x^6$, respectively. In the cooperative communication environment, the signal-to-noise ratio (SNR) of S_1-D, S_2-D, and S_1-S_2 links are expressed as $\gamma_{S_1,D}$, $\gamma_{S_2,D}$ and γ_{S_1,S_2}, respectively. The optimal detection is realized through the MLD method. It should be noted that the MLD strategy intrinsically accomplishes channel compensation during its optimal decision process, thereby rendering a separate equalization algorithm unnecessary. Perfect channel state information and ideal S_1–S_2 link are supposed for the dual benefits of reducing simulation time and better clarifying the impact of system parameters on error performance. Non-ideal S_1–S_2 channel conditions are introduced to evaluate the impact of realistic inter-source link constraints on system error performance. Table 3 presents the primary simulation parameters for the proposed NC-RSCC-MIMO system under three different scenarios defined in Tab. 2, where $\gamma_{S_2,D} \le \gamma_{S_1,D} + 2$ dB is chosen to reduce the runtime, $n_r \le 6$ is constrained to simplify the receiver configuration, and the modulation order M for M-QAM is determined by the number of elements in $GF(2^m)$, i.e., $M = 2^m$. All the numerical experiments are conducted in MATLAB. The following simulated results are ultimately presented as the BER performance curves versus SNR ($\gamma_{S_1,D}$).

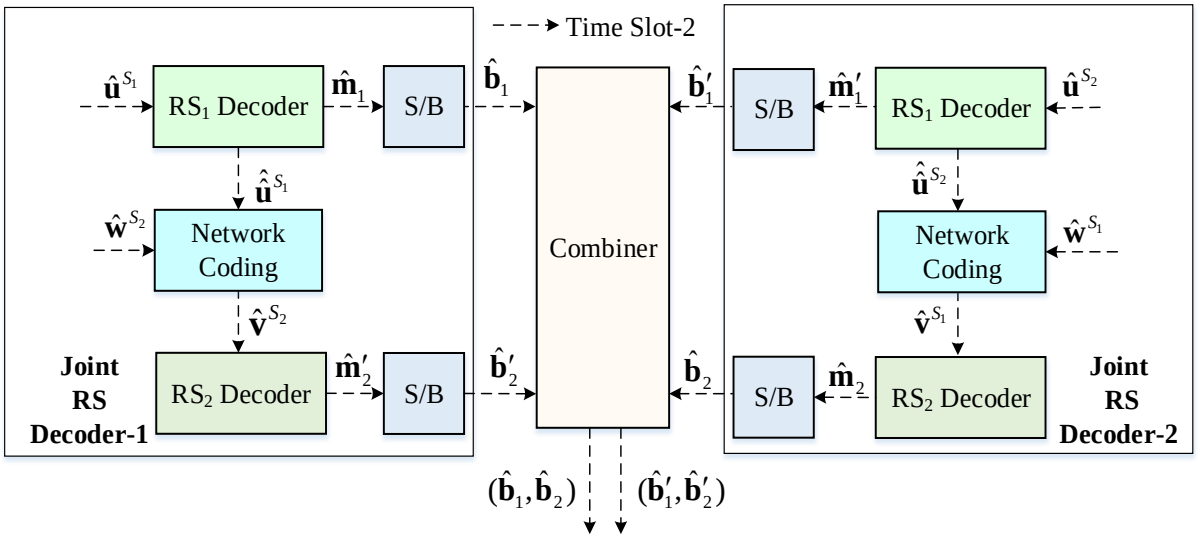

Fig. 2. Parallel joint RS decoding in the destination.

Scenarios	RS code pairs $RS_1(N_1, K_1, d_1)$, $RS_2(N_2, K_2, d_2)$	Optimized NCCCs	Fields	Fields' primitive polynomials over GF(2)
M_1	$RS_1(15,3,13)$, $RS_2(15,2,14)$	$\alpha_{OPT}=(\beta,\beta)$, $\alpha_{LC}=(\beta^{10},\beta^{10})$	$GF(2^4)=\{0,1,\beta,...,\beta^{14}\}$	$1+x+x^4$
M_2	$RS_1(31,11,21)$, $RS_2(31,8,24)$	$\alpha_{LC}=(\lambda^3,\lambda)$	$GF(2^5)=\{0,1,\lambda,...,\lambda^{30}\}$	$1+x^2+x^5$
M_3	$RS_1(63,28,36)$, $RS_2(63,20,44)$	$\alpha_{LC}=(\eta^2,\eta^2)$	$GF(2^6)=\{0,1,\eta,...,\eta^{62}\}$	$1+x+x^6$

Tab. 2. Optimized NCCCs and the relevant parameters for the three scenarios.

Scenarios	Channel models	Relationship between $\gamma_{S_1,D}$ and $\gamma_{S_2,D}$	MIMO setups	Modulation	Equivalent code rates in destination	Detection	Decoding
M_1	slow/fast Rayleigh fading channel	$\gamma_{S_2,D}=\gamma_{S_1,D}$ $\gamma_{S_2,D}=\gamma_{S_1,D}+1$ dB $\gamma_{S_2,D}=\gamma_{S_1,D}+2$ dB	$n_r=4,6$	16-QAM (M = 16)	5/30	MLD	proposed parallel joint decoding
M_2	slow/fast Rayleigh fading channel	$\gamma_{S_2,D}=\gamma_{S_1,D}+2$ dB	$n_r=3,4,5,6$	32-QAM (M = 32)	19/62	MLD	proposed parallel joint decoding
M_3	slow/fast Rayleigh fading channel	$\gamma_{S_2,D}=\gamma_{S_1,D}+2$ dB	$n_r=4,6$	64-QAM (M = 64)	48/126	MLD	proposed parallel joint decoding

Tab. 3. Simulation parameters.

5.1 Impact of Varying NCCC Selection Algorithms on the NC-RSCC-MIMO System

Figure 3 gives the impact of different NCCC selection algorithms on the BER of NC-RSCC-MIMO system in scenario M_1 over slow Rayleigh fading channel. This SNR of S_1-S_2 link is assumed to be infinite ($\gamma_{S_1,S_2}=\infty$, i.e., noise-free or ideal), with $\gamma_{S_2,D}=\gamma_{S_1,D}+2$ dB employed. By applying the two proposed optimized NCCC selection algorithms (i.e., ONCCCS and LC-ONCCCS), the resulting optimized NCCCs are obtained, as presented in Tab. 2. Simulation results indicate that the system performance is very close between the LC-ONCCCS and ONCCCS algorithms across the entire SNR range. The observed phenomenon results from both algorithms' ability to generate equivalent linear block codes exhibiting the same minimum distance (i.e., 20) at the destination, showing the LC-ONCCCS algorithm enables to achieve optimized code-

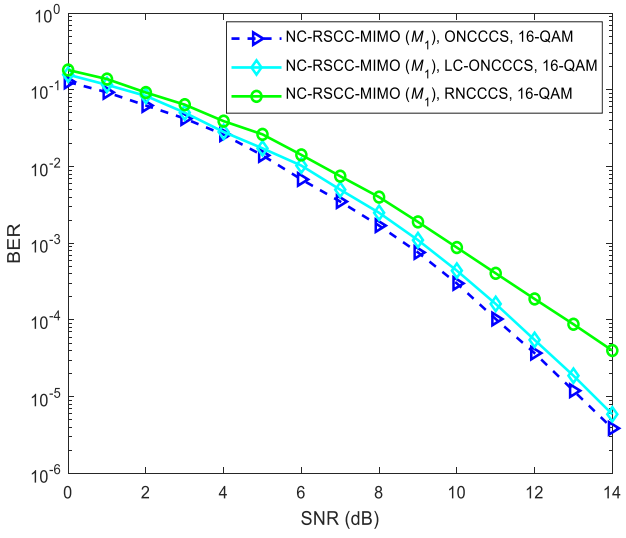

Fig. 3. Performance comparison of various NCCC selection algorithms in the NC-RSCC-MIMO system under scenario M_1 with 16-QAM and $n_r=4$.

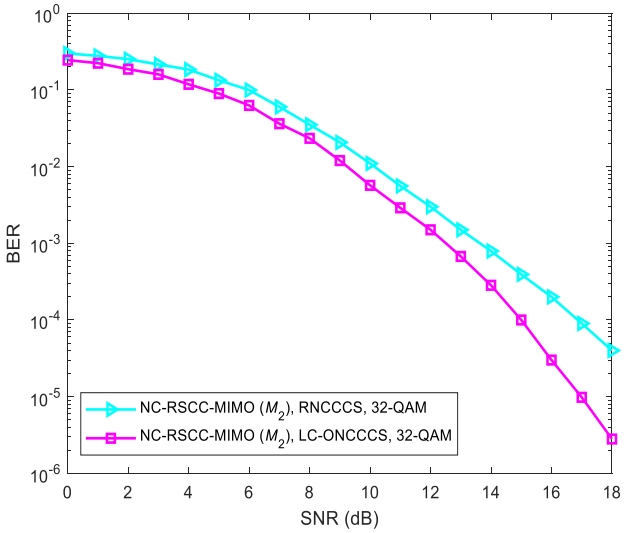

Fig. 4. Performance comparison of various NCCC selection algorithms in the NC-RSCC-MIMO system under scenario M_2 with 32-QAM and $n_r=4$.

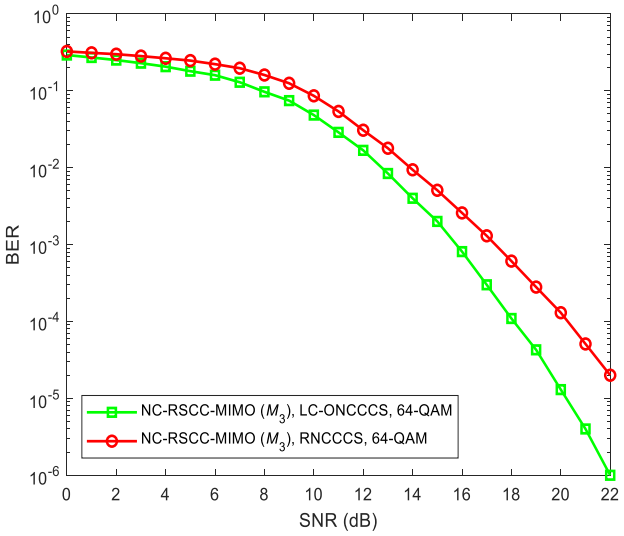

Fig. 5. Performance comparison of various NCCC selection algorithms in the NC-RSCC-MIMO system under scenario M_3 with 64-QAM and $n_r = 4$.

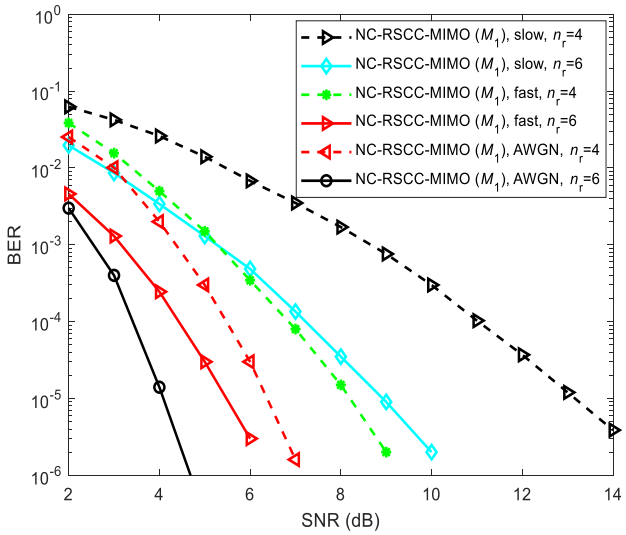

Fig. 6. Performance curves of the NC-RSCC-MIMO system in scenario M_1 over different channels with 16-QAM.

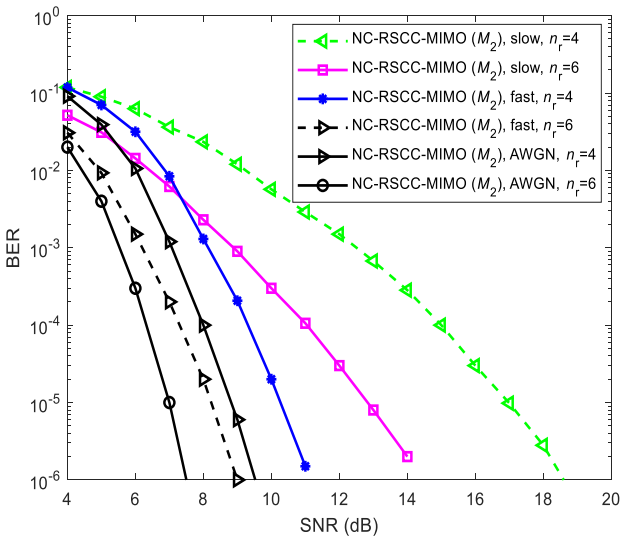

Fig. 7. Performance curves of the NC-RSCC-MIMO system in scenario M_2 over different channels with 32-QAM.

word weight distribution and verifying it is able to realize compromise between the computational efficiency and achievable error performance. Furthermore, in Fig. 3, the quantitative performance comparison with the random NCCC selection (RNCCCS) algorithm generating the small free distance (i.e., 15) shows that both the proposed ONCCCS and LC-ONCCCS algorithms deliver significant error performance enhancement via codeword weight optimization in the constructed equivalent codes at the receiver. At BER = 4×10^{-5}, the NC-RSCC-MIMO system gains roughly 2 dB and 1.75 dB SNR improvement using the ONCCCS and LC-ONCCCS algorithms compared to the RNCCCS algorithm.

The LC-ONCCCS algorithm achieves a better balance between complexity and error performance, demonstrating particular suitability for scenarios M_2 and M_3 characterized by longer information block lengths and more field elements. The system performance employing this algorithm is illustrated in Figs. 4 and 5, with the optimized NCCCs for scenarios M_2 and M_3 detailed in Tab. 2. The conditions $\gamma_{S_2,D} \leq \gamma_{S_1,D} + 2$ dB and $\gamma_{S_1,S_2} = \infty$ are supposed. The results in Figs 4 and 5 also demonstrate a notable enhancement in performance when employing the LC-ONCCCS algorithm as opposed to the conventional RNCCCS approach.

5.2 Error Performance of the NC-RSCC-MIMO System under Different Channels

This subsection evaluates the BER performance of the NC-RSCC-MIMO system in scenarios M_1, M_2 and M_3 over slow Rayleigh fading, fast Rayleigh fading and AWGN channels, where $\gamma_{S_1,S_2} = \infty$ and $\gamma_{S_2,D} \leq \gamma_{S_1,D} + 2$ dB are utilized. The scenario M_1 employs the optimal NCCC generated by the ONCCCS algorithm, while the scenarios M_2 and M_3 utilize the optimized NCCCs obtained by the LC-ONCCCS algorithm, as displayed in Tab. 2. The comparative analysis of the system BER performance gap between the AWGN and fading channels in Figs. 6-8 exhibits the performance superiority of the AWGN channel, which benefits from the absence of fading in contrast to the random signal attenuation inherent to fading channels. Furthermore, against the AWGN channel benchmark, we quantitatively demonstrate that the fast fading condition yields better performance than the slow fading condition. This performance enhancement stems from the rapid channel variations in fast fading environments, which induces statistically independent fading across successive time intervals. The resulting channel fading independence effectively compensates for the channel-induced signal degradation, thereby improving the system's performance.

Figure 6 shows that the NC-RSCC-MIMO system separately achieves 4.9 dB and 1.4 dB gains over AWGN channel compared to slow and fast Rayleigh fading channels at BER = 10^{-5} with $n_r = 6$, indicating that the fast fading condition exhibits a 3.5 dB advantage over the slow

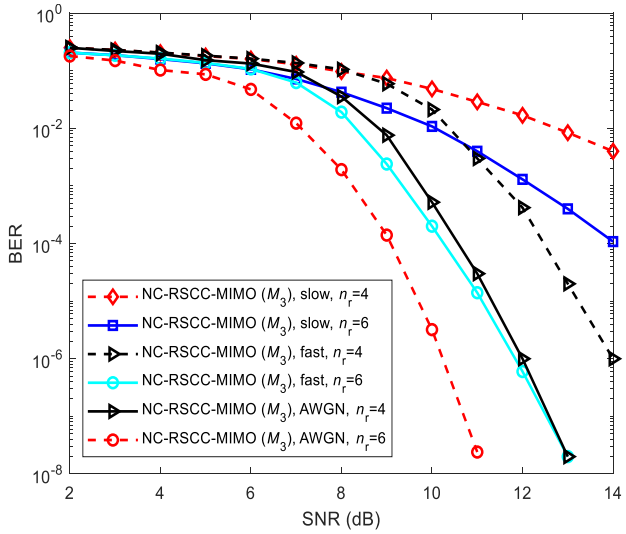

Fig. 8. Performance curves of the NC-RSCC-MIMO system in scenario M_3 over different channels with 64-QAM.

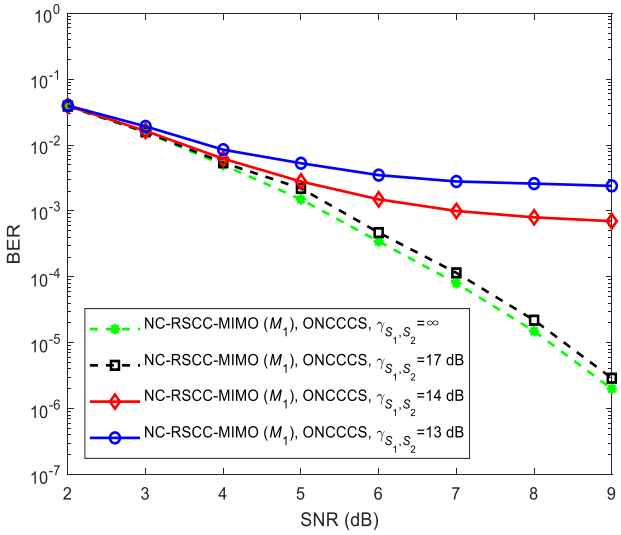

Fig. 9. Error performance of the NC-RSCC-MIMO system in scenario M_1 under different S_1-S_2 link conditions with 16-QAM and $n_r = 4$.

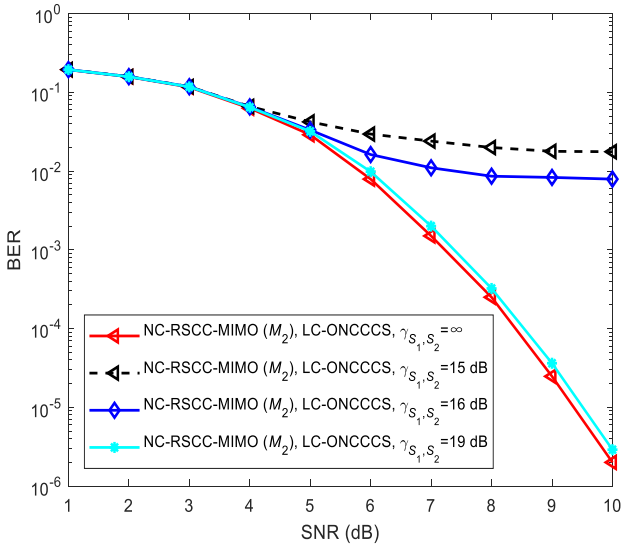

Fig. 10. Error performance of the NC-RSCC-MIMO system in scenario M_2 under different S_1-S_2 link conditions with 32-QAM and $n_r = 5$.

fading condition. Figures 7 and 8 further validate this trend: 1) In Fig. 7 at BER = 10^{-5} with $n_r = 6$, the corresponding gains of the AWGN channel are 5.8 dB and 1.25 dB, resulting in a 4.55 dB gain for fast fading. 2) In Fig. 8 at BER = 10^{-4} with $n_r = 6$, the respective gains are 4.9 dB and 1.2 dB, yielding a 3.7 dB gain for fast fading.

5.3 Influence of Various SNRs between Two Sources on the NC-RSCC-MIMO System

Under the SNR of S_1-S_2 link satisfies $\gamma_{S_1,S_2} = \infty$ (ideal), each source node can perfectly decode the information from the other. However, in practical scenarios, the inter-source links generally operate under non-ideal conditions (i.e., $\gamma_{S_1,S_2} \neq \infty$). Thus, this subsection conducts a comparative performance analysis of the NC-RSCC-MIMO system under various S_1-S_2 link conditions.

Figures 9–11 demonstrate the impact of different values of γ_{S_1,S_2} on the BER performance of the NC-RSCC-MIMO system in these scenarios M_1, M_2 and M_3, where fast Rayleigh fading channel and $\gamma_{S_2,D} = \gamma_{S_1,D} + 2$ dB are employed. In scenarios M_1, M_2 and M_3, the optimized NCCC selection patterns generated by the ONCCCS, LC-ONCCCS and LC-ONCCCS algorithms are separately used and the detailed parameters are provided in Tab. 2. Simulation results reveal that under the bad S_1-S_2 link conditions (i.e., $\gamma_{S_1,S_2} = 13$ dB and 14 dB for scenario M_1, $\gamma_{S_1,S_2} = 15$ dB and 16 dB for scenario M_2, and $\gamma_{S_1,S_2} = 19$ dB and 20 dB for scenario M_3), the system exhibits degraded performance and encounters an error floor at high SNR. This phenomenon arises from decoding errors at the source node, inducing uncontrolled error propagation along the transmission path. This issue can be effectively mitigated through implementation of a cyclic redundancy check (CRC) technology. Notably, when this S_1-S_2 link increases to higher level (i.e., $\gamma_{S_1,S_2} = 17$ dB for scenario M_1, $\gamma_{S_1,S_2} = 19$ dB for scenario M_2, and $\gamma_{S_1,S_2} = 23$ dB for scenario M_3), the performance difference between the practical operating conditions and the ideal case ($\gamma_{S_1,S_2} = \infty$) diminishes significantly. As depicted in Fig. 9, the system under favorable S_1-S_2 link condition (i.e., $\gamma_{S_1,S_2} = 17$ dB) exhibits only 0.2 dB degradation relative to the ideal case at BER = 2.9×10^{-6}. Similarly, Figures 10 and 11 separately demonstrate performance gaps of 0.16 dB and 0.16 dB under high-quality S_1-S_2 link conditions when compared with the ideal scenario ($\gamma_{S_1,S_2} = \infty$) at BER = 10^{-5}. These experimental findings robustly validate the proposed NC-RSCC-MIMO system can achieve exceptional performance in practical applications with well-conditioned S_1-S_2 links.

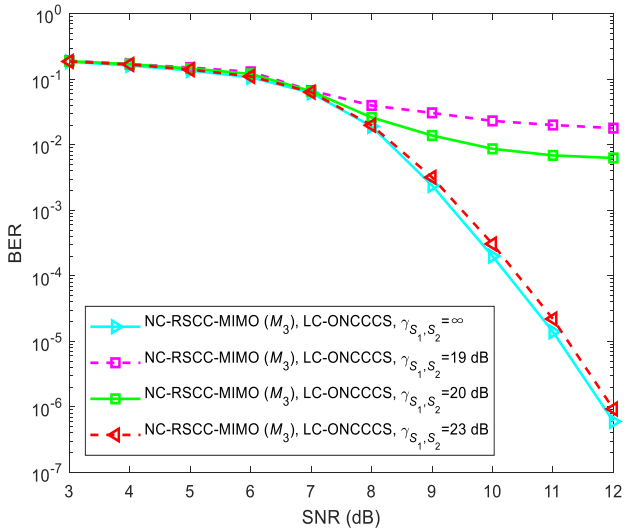

Fig. 11. Error performance of the NC-RSCC-MIMO system in scenario M_3 under different S_1-S_2 link conditions with 64-QAM and $n_r = 6$.

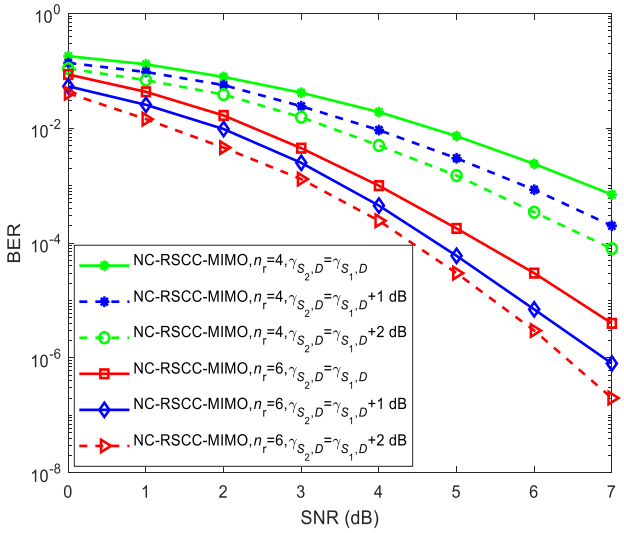

Fig. 12. Effect of various S_2-D link conditions on the NC-RSCC-MIMO system BER performance in scenario M_1 with 16-QAM.

5.4 Performance Comparison of the NC-RSCC-MIMO System under Different S_2-D Link Conditions

Figure 12 presents the BER performance evaluation of the NC-RSCC-MIMO system in scenario M_1 over fast Rayleigh fading channel, examining the impact of different S_2-D link conditions (represented by the values of $\gamma_{S_2,D}$) on system performance, in which higher $\gamma_{S_2,D}$ indicates the shorter S_2-D distance compared to the S_1-D link. The parameter configuration $\gamma_{S_1,S_2} = \infty$ and the optimal NCCC from Tab. 2 are adopted.

Due to the full exploitation of the additional SNR gain at the source node S_2, it enables to get more reliable joint signal detection and consequent system improvements compared to its counterparts, where the case $\gamma_{S_2,D} = \gamma_{S_1,D}$ in Fig. 12 denotes the non-cooperative scenario. For instance: 1) For $n_r = 4$ at BER = 7×10^{-4}, the $\gamma_{S_2,D} = \gamma_{S_1,D} + 2$ dB case gets 1 dB and 1.5 dB gains relative to the cases $\gamma_{S_2,D} = \gamma_{S_1,D} + 1$ dB and $\gamma_{S_2,D} = \gamma_{S_1,D}$ (non-cooperative case), respectively. 2) For $n_r = 6$ at BER = 4×10^{-6}, these SNR gains are about 0.75 dB and 1.1 dB, respectively.

5.5 Impact of Various Receive Antenna Number on the NC-RSCC-MIMO System

Figures 13 and 14 present a comparative BER of the NC-RSCC-MIMO system in scenario M_2 with varying receive antenna number n_r, under the assumptions $\gamma_{S_2,D} = \gamma_{S_1,D} + 2$ dB and $\gamma_{S_1,S_2} = \infty$. The adopted optimized NCCC yielded by the LC-ONCCCS algorithm is listed in Tab. 2. The experimental results show progressive enhancement with each additional antenna. This achieved performance boost originates from enhanced spatial diversity gain facilitated by the incorporation of extra receive

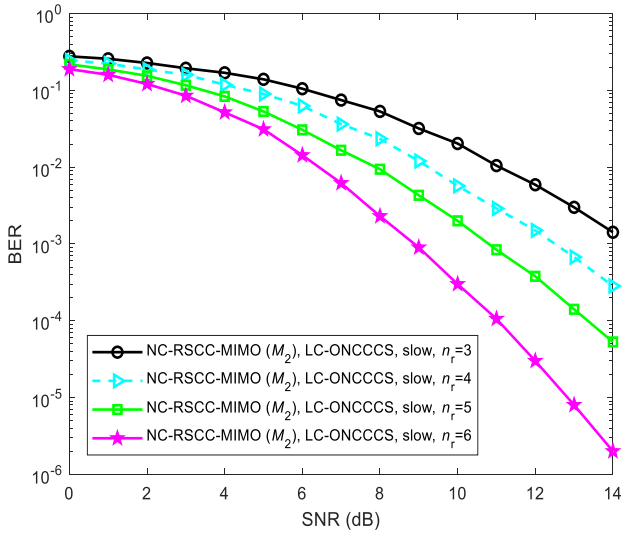

Fig. 13. Performance impact of different receive antenna number n_r on the NC-RSCC-MIMO system in scenario M_2 over slow Rayleigh fading channel with 32-QAM.

antennas. For example, Figure 13 presents that the BER performance is 1.4×10^{-3} for $n_r = 3$, while separately improving to 2.8×10^{-4}, 5.3×10^{-5} and 2×10^{-6} for $n_r = 4$, 5, and 6 at SNR=14 dB. Figure 14 shows the corresponding BER is 3.6×10^{-3}, 2.1×10^{-4}, 2.5×10^{-5} and 10^{-6} for $n_r = 3$, 4, 5 and 6 at SNR = 9 dB.

The computation time of the simulations relies on the parameter values. For the results presented in Fig. 13, the computation times are as follows: 1) 1.3 hours for $n_r = 3$. 2) 1.4 hours for $n_r = 4$. 3) 1.41 hours for $n_r = 5$. 4) 1.42 hours for $n_r = 6$. It can be observed that increasing the number of antennas slightly adds the runtime required. Furthermore, this section analyzes the computational complexity of the proposed NC-RSCC-MIMO system. The analysis primarily focuses on the detection complexity at the destination, as the variation in overall system complexity

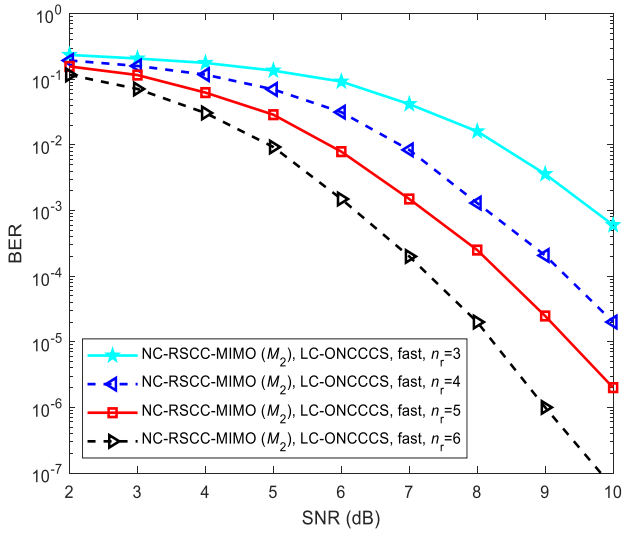

Fig. 14. Performance impact of different receive antenna number n_r on the NC-RSCC-MIMO system in scenario M_2 over fast Rayleigh fading channel with 32-QAM.

ty under different n_r is predominantly reflected in the processing of the destination. Specifically, the detection complexity φ_D at the destination is expressed as the sum of the MLD complexity φ_{MLD} and the parallel joint RS decoding complexity φ_{DEC}, i.e., $\varphi_D = \varphi_{MLD} + \varphi_{DEC}$. In the complexity analysis, the addition and multiplication operations are taken into account, thus getting the related expressions $\varphi_{MLD} = 2(N_1 + N_2)(3n_r + 2M - 1)$ and $\varphi_{DEC} = 4M(\log_2(M))^2$. For example, with $N_1 = N_2 = 31$ and $M = 32$, the value of φ_D is 12128 for $n_r = 3$ and increases to 13244 for $n_r = 6$. Compared to the configuration with $n_r = 3$, the slight increase of 8.4% in computational complexity is observed for the case with $n_r = 6$.

Based on runtime and complexity analysis, the proposed NC-RSCC-MIMO system exhibits excellent scalability as the number of receive antennas increases, demonstrating only marginal growth in both runtime and computational load. This favorable scaling characteristic indicates strong hardware feasibility by enabling efficient implementation on general-purpose processors without requiring costly specialized hardware. Furthermore, the deterministic operational procedures of the parallel joint RS decoding architecture ensure consistently low decoding latency, making the system well-suited for the fifth generation (5G) real-time communication applications.

5.6 Performance Comparison of the NC-RSCC-MIMO System versus the Existing Systems

Figure 15 compares the proposed NC-RSCC-MIMO system (M_1 scenario with optimal NCCC from Tab. 2) against five state-of-the-art systems over slow Rayleigh fading channel, i.e., RS coded cooperative SM (RSCC-SM) [20], reconfigurable intelligent surface (RIS) assisted LDPC coded cooperation (RIS-LDPCCC) [21], RIS assisted polar coded cooperation (RIS-PCC) [22], Goppa coded cooperative generalized SM (GCC-GSM) [23] and distributed generalized RS coded generalized SM (DGRSC-GSM) [24] under the identical spectral efficiency and code rate.

The evaluation uses $\gamma_{S_1,S_2} = \infty$, $\gamma_{S_2,D} = \gamma_{S_1,D} + 2$ dB and MLD method. The corresponding spectral efficiencies of the NC-RSCC-MIMO system, GSM-based systems and other comparative systems are separately $\log_2(n_t M)$, $0.5\left\lfloor \log_2(C_{n_t}^{n_u}) \right\rfloor + 0.5\log_2(M)$ and $0.5\log_2(n_t M)$, where n_t and M are separately the transmit antenna number and modulation order of each system, and n_u ($n_u \le n_t$) is the active transmit antenna number of GSM-based systems. Note that in the NC-RSCC-MIMO and the RIS-aided systems, the number of transmit antennas is set to one, i.e., $n_t = 1$. Since the NC-RSCC-MIMO system in scenario M_1 is considered, its spectral efficiency is $\log_2(16) = 4$ bits/s/Hz. For realizing the same spectral efficiency of 4 bits/s/Hz, the RIS-aided systems utilize 256-QAM and $n_t = 1$, the RSCC-SM system uses 16-QAM and $n_t = 16$, whereas the GSM-based systems employ 16-QAM, $n_t = 7$ and $n_u = 2$. To maintain a consistent equivalent code rate of 5/30 at the destination, four equivalent coding schemes are employed: 1) The RSCC-based systems and the DGRSC-GSM system employs the (30, 5) non-binary code. 2) The RIS-LDPCCC system uses the (120, 20) binary LDPC code. 3) The RIS-PCC system adopts the (128, 22) binary polar code, where the selected 128-bit codeword length fulfills the power-of-two constraint while providing a close approximation to desired 120-bit target length. 4) The GCC-GSM system employs the (120, 20) binary Goppa code. Also, three distinct decoding methods are implemented:

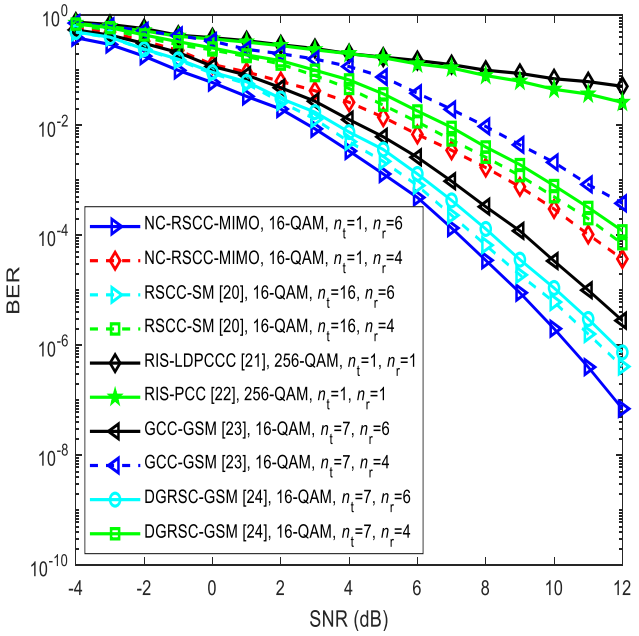

Fig. 15. Performance comparison of the NC-RSCC-MIMO system in scenario M_1, RSCC-SM [20], RIS-aided systems (i.e., RIS-LDPCCC [21] and RIS-PCC [22]) with 12 reflecting elements, GCC-GSM [23] and DGRSC-GSM [24].

1) The RSCC-based and GSM-based systems employ joint decoding based on Euclidean algorithm. 2) The RIS-LDPCCC scheme utilizes 12-iteration belief propagation decoding. 3) The RIS-PCC scheme uses CRC aided successive cancellation list decoding, incorporating list size of $L = 32$ and 16-bit CRC.

Experimental evaluations confirm the superior performance of the proposed NC-RSCC-MIMO system compared to the SM-based and GSM-based systems with the same n_r, and other RIS-assisted systems at high SNR. This is attributed to three key innovations, i.e., MIMO diversity exploitation, optimal network coding strategy and efficient parallel joint decoding technique. For example, the proposed system under $n_r = 6$ demonstrates performance gains of more than 1 dB over the existing systems at BER = 4.1×10^{-7}.

6. Conclusion

This manuscript proposes a novel dual-source single-destination NC-RSCC-MIMO system that innovatively utilizes RS codes at both source nodes to simultaneously achieve coded cooperation and network coding. In the NC-RSCC-MIMO system, the selection strategy of NCCC critically determines the codeword weight distribution in the destination. While the proposed ONCCCS algorithm can achieve optimal system performance, it incurs prohibitively high complexity when processing large field sizes and long information sequences. To address the performance-complexity trade-off, this paper develops the LC-ONCCCS algorithm that maintains comparable error performance to the ONCCCS while significantly reducing computational overhead. Furthermore, an efficient parallel joint RS decoding approach is implemented. Experimental results show that the LC-ONCCCS algorithm delivers performance nearly identical to the ONCCCS algorithm and it also demonstrates substantial improvements over the traditional RNCCCS. Compared with non-cooperative systems, the proposed NC-RSCC-MIMO scheme exhibits remarkable performance gains. Most notably, the proposed NC-RSCC-MIMO system effectively integrates three key technical advantages (i.e., MIMO spatial diversity, optimized network coding and parallel joint decoding), ultimately achieving superior performance over existing solutions. The NC-RSCC-MIMO framework has rapid encoding/decoding and enhanced BER performance, thus being able to better satisfy the requirements of 5G ultra-reliable low-latency communications. The demonstrated reliability and spectral efficiency make the proposed NC-RSCC-MIMO system particularly suitable for potential application scenarios such as vehicular networks and D2D communication, where robust link quality and low latency are paramount. Future work will address near-optimal NCCC selection algorithm and joint decoding optimization.

Acknowledgments

Funding: This work was supported by Doctoral Research Start-up Foundation of Henan University of Technology (No. 2024BS031).

Data Availability Statement: All the source codes and mathematical models are available from the authors upon reasonable request.

References

[1] CHU, Z., ZHOU, F. H., ZHU, Z. Y., et al. Energy beamforming design and user cooperation for wireless powered communication networks. *IEEE Wireless Communications Letters*, 2017, vol. 6, no. 6, p. 750–753. DOI: 10.1109/LWC.2017.2739148

[2] LI, K. K., TAO, M. X., ZHANG, J. J., et al. Coded computing and cooperative transmission for wireless distributed matrix multiplication. *IEEE Transactions on Communications*, 2021, vol. 69, no. 4, p. 2224–2239. DOI: 10.1109/TCOMM.2021.3053018

[3] DING, W. H., BAHAEI, M. S. A partial compress-and-forward strategy for relay-assisted wireless networks based on rateless coding. *IEEE Transactions on Vehicular Technology*, 2024, vol. 73, no. 1, p. 1462–1466. DOI: 10.1109/TVT.2023.3310771

[4] YANG, J., ZHU, C. H., GUO, X. Y., et al. Partial cooperation based on dynamic transmit antennas for two-hop massive MIMO systems. *Wireless Communications and Mobile Computing*, 2018, no. 1, p. 1–7. DOI: 10.1155/2018/4578059

[5] HUNTER, T. E., NOSRATINIA, A. Diversity through coded cooperation. *IEEE Transactions on Wireless Communications*, 2006, vol. 5, no. 2, p. 283–289. DOI: 10.1109/TWC.2006.02006

[6] UMAR, R., YANG, F. F., XU, H. J., et al. Distributed turbo coded spatial modulation based on code matched interleaver for MIMO system. *Wireless Networks*, 2023, vol. 29, no. 5, p. 1995–2013. DOI: 10.1007/s11276-023-03256-1

[7] ZHAO, C. L., YANG, F. F., WAWERU, D. K., et al. Distributed QC-LDPC coded spatial modulation for half-duplex wireless communications. *Radioengineering*, 2022, vol. 31, no. 3, p. 362–373. DOI: 10.13164/re.2022.0362

[8] CHEN, C., YANG, F. F., XU, H. J. Jointly optimized quasi-cyclic LDPC codes for coded-cooperative wireless networks based on split labeling diversity. *Telecommunication Systems*, 2024, vol. 85, no. 3, p. 461–476. DOI: 10.1007/s11235-024-01102-z

[9] LIANG, H., LIU, A. J., LIU, X., et al. Construction and optimization for adaptive polar coded cooperation. *IEEE Wireless Communications Letters*, 2020, vol. 9, no. 8, p. 1187–1190. DOI: 10.1109/LWC.2020.2984738

[10] LIANG, H., LIU, A. J., DAI, J. C., et al. Design and analysis of polar coded cooperation with incremental redundancy for IoT in fading channels. *IET Communications*, 2021, vol. 15, no. 4, p. 595–602. DOI: 10.1049/cmu2.12091

[11] ZHAO, P., FENG, L., YU, P., et al. Joint power allocation and subcarrier assignment for device to device in 5G time division duplex networks. *International Journal of Distributed Sensor Networks*, 2018, vol. 14, no. 11. DOI: 10.1177/1550147718811094

[12] ZHAO, P., GUO, W. L., XU, D. T., et al. Hypergraph-based resource allocation for device-to-device underlay H-CRAN

network. *International Journal of Distributed Sensor Networks*, 2020, vol. 16, no. 8. DOI: 10.1177/1550147720951337

[13] YANG, B., TALEB, T., SHEN, Y. L., et al. Performance, fairness, and tradeoff in UAV swarm underlaid mmWave cellular networks with directional antennas. *IEEE Transactions on Wireless Communications*, 2021, vol. 20, no. 4, p. 2383–2397. DOI: 10.1109/TWC.2020.3041800

[14] FAN, Y. J., GAO, S. J., DUAN, D. L, et al. Radar integrated MIMO communications for multi-hop V2V networking. *IEEE Wireless Communications Letters*, 2023, vol. 12, no. 2, p. 307–311. DOI: 10.1109/LWC.2022.3224566

[15] WU, Y. S. Twisted Reed-Solomon codes with one-dimensional hull. *IEEE Communications Letters*, 2021, vol. 25, no. 2, p. 383–386. DOI: 10.1109/LCOMM.2020.3025178

[16] AL-MOLIKI, Y. M., ALDHAEEBI, M. A., ALMWALD, G. A., et al. The performance of RS and RSCC coded cooperation systems using higher order modulation schemes. In *Proceedings of 6th International Conference on Intelligent Systems, Modelling and Simulation*. Kuala Lumpur (Malaysia), 2015, p. 211–214. DOI: 10.1109/ISMS.2015.11

[17] GUO, P. C., YANG, F. F., ZHAO, C. L., et al. Jointly optimized design of distributed Reed-Solomon codes by proper selection in relay. *Telecommunication Systems*, 2021, vol. 78, no. 3, p. 391–403. DOI: 10.1007/s11235-021-00822-w

[18] CHEN, C., YANG, F. F., ZHAO, C. L., et al. Distributed RS coded cooperation: Optimized code construction and decoding by critical SNR aided. *Wireless Personal Communications*, 2023, vol. 132, no. 1, p. 523–548. DOI: 10.1007/s11277-023-10623-w

[19] ZHAO, C. L., YANG, F. F., WAWERU, D. K. Reed-Solomon coded cooperative spatial modulation based on nested construction for wireless communication. *Radioengineering*, 2021, vol. 30, no. 1, p. 172–183. DOI: 10.13164/re.2021.0172

[20] ZHAO, C. L., YANG, F. F., ULLAH, W. Jointly optimized design of distributed RS-coded spatial modulation by appropriate selection at the relay. *Eurasip Journal on Wireless Communications and Networking*, 2023, vol. 2023, no. 1, p. 1–29. DOI: 10.1186/s13638-023-02211-0

[21] WANG, J., ZHANG, S. W., MEI, Z. H., et al. RIS-assisted coded relay cooperation based on LDPC product codes with finite code length. In *Proceedings of International Conference on Wireless Communications and Signal Processing (WCSP)*. Hangzhou, (China), 2023, p. 1038–1043. DOI: 10.1109/WCSP58612.2023.10405032

[22] PAN, Y., ZHANG, S. W. Performance analysis of RIS-assisted coded cooperation system based on polar codes with finite code length. *IEEE Signal Processing Letters*, 2024, vol. 31, p. 2290–2294. DOI: 10.1109/LSP.2024.3453662

[23] CHEN, C., YANG, F. F., WAWERU, D. K. Optimized-Goppa codes based on the effective selection of Goppa polynomials for coded-cooperative generalized spatial modulation network. *Radioengineering*, 2024, vol. 33, no. 1, p. 75–88. DOI: 10.13164/re.2024.0075

[24] ZHAO, C. L., YANG, F. F., XU, H. J. Optimized design of distributed generalized Reed-Solomon coded generalized spatial modulation. *Radioengineering*, 2025, vol. 34, no. 2, p. 273–288. DOI: 10.13164/re.2025.0273

About the Authors ...

Chunli ZHAO (corresponding author) received her B.S. degree in Electronic and Information Engineering from Henan Normal University Xinlian College, China, in 2014. She obtained her M.Sc. degree in Circuits and Systems at Henan Normal University, China, in 2017. She received her Ph.D. degree in Communication and Information Systems from Nanjing University of Aeronautics and Astronautics, China, in 2024. She is currently a lecturer with the College of Information Science and Engineering at Henan University of Technology. Her research interests include channel coding, coded cooperation and MIMO technique.

Fengfan YANG received the M.Sc. and Ph.D. degrees from the Northwestern Polytechnical University and South-east University, China in 1993, and 1997, respectively, all in Electronic Engineering. He has been with the College of Information Science and Technology, Nanjing University of Aeronautics and Astronautics since May 1997. From October 1999 to May 2003, he was a research associate at the Centre for Communication Systems Research, University of Surrey, UK, and Dept. of Electrical and Computer Engineering, McGill University, Canada. His major research interests are information theory, channel coding and their applications for mobile and satellite communications.

Binkun LIU received the B.Sc. degree from the Henan University of Science and Technology, Luoyang, China, in 2015. He obtained the M.Sc. degree from the Dalian Jiaotong University, Dalian, China, in 2017. He is currently working in the College of Information Science and Engineering, Henan University of Technology. His research direction is wireless communication.

Hongjun XU (MIEEE, 07) received the B.Sc. degree from the University of Guilin Technology, Guilin, China, in 1984; the M.Sc. degree from the Institute of Telecontrol and Telemeasure, Shi Jian Zhuang, China, in 1989; and the Ph.D. degree from the Beijing University of Aeronautics and Astronautics, Beijing, China, in 1995. From 1997 to 2000, he was a Postdoctoral Fellow with the University of Natal, Durban, South Africa, and Inha University, Incheon, Korea. He is currently a full Professor with the School of Engineering at the University of KwaZulu-Natal, Durban. He is also a rated scientist of the national research foundation in South Africa. He has authored and co-authored more than 50 journal papers. His research interests include wireless communications and image processing.